Role of surface wetting on tribological behavior for laser nanotextured steel using ionic liquid lubricants

Avik Samanta [a],[1], Wuji Huang [b],[1], Kyungjun Lee [c], Xin He [d], Chanaka Kumara [d], Jun Qu [d], Hongtao Ding [b],[*]

[a] *Energy and Environment Directorate, Pacific Northeast National Laboratory, Richland, WA 99354, USA*
[b] *Department of Mechanical Engineering, The University of Iowa, Iowa City, IA 52242, USA*
[c] *Division of Mechanic Smart Industrial Engineering, Gachon University, Seongnam 13120, Republic of Korea*
[d] *Materials Science and Technology Division, Oak Ridge National Laboratory, Oak Ridge, TN 37831, USA*

ARTICLE INFO

ABSTRACT

This research evaluates the effect of surface wettability on the tribological performance through ball-on-flat tribology testing. The substrate material, M2 tool steel, is laser processed and then functionalized with fluoro-carbon and nitrile chemistry to achieve distinct oleophobicity and oleophilicity, respectively, but with a similar nanoscale surface texture. The baseline lubricant is poly-alpha-olefin (PAO) oil, and ionic liquids (ILs) are used as additives for this study. The interaction between the nanoscale textured steel surface and ionic liquid-based oils is investigated. A set of reciprocating wear tests are performed to investigate the tribological behavior of the tribo-system consisting of the surface-engineered, flat M2 tool steel specimen and a standard, surface-polished steel ball. Results show that the oleophobic flat surface results in a lower friction, while the oleophilic surface modification leads to a better wear protection to the flat surface. Ammonium-based IL provides the highest friction reduction, while the phosphonium-based ILs provide an improved wear protection.

1. Introduction

Lubrication study has been attracting interests as potential savings of up to 1.4 % of a nation's GDP can be accomplished by friction and wear reduction of moving components [1]. Though not all friction can be eliminated, mechanical losses can be minimized by applying high performance lubricants and optimizing the tribological properties through surface modification. For instance, most mechanical losses in electric motors in electrical vehicles (EV) come from frictional bearing losses [2], and 40–60 % of premature electric motor failures are caused by bearings and improper lubrication [3], limiting vehicle range. The EV industry in particular has been increasingly exploring lubrication and surface engineering solutions to reduce friction due to higher rotational speeds and demanding conditions on the bearings used in EV transmissions [4]. Developing an understanding of the tribological behaviors and mechanisms of surfaces interaction under oil lubrication is crucial to this endeavor.

The tribological performance of contacting surfaces under lubrication can be influenced by both the surface properties and lubricant properties. Surface engineering methods have been explored to improve tribological performance by modifying surface properties, among which laser texturing is commonly used [5–9]. Efforts have been made to generate micro-scale geometric features on tribo-surfaces including micro-grooves [10,11] and micro-dimples [12–14] via laser texturing. Researchers found that those surface features help improve lubrication as they provide a local reservoir for lubricants in the boundary lubrication condition, and the surface features will squeeze the lubricant out when other parts or surfaces press the textured surface resulting in secondary lubrication [15]. Therefore, a reduced coefficient of friction (COF) for both oil and water lubrication and improved wear resistance will be achieved. The surface texturing parameters, such as areal density, dimple shape, size, and depth were also studied to achieve desired friction reduction [16]. However, most of the existing laser-assisted tribology research focused on surface morphology and its effect on tribology. The effect of wettability of laser-processed metal surface on the tribological performance was not thoroughly investigated.

Surface wettability plays an important role in the tribological performance of tribo-pair surfaces under lubrication, as it will affect the
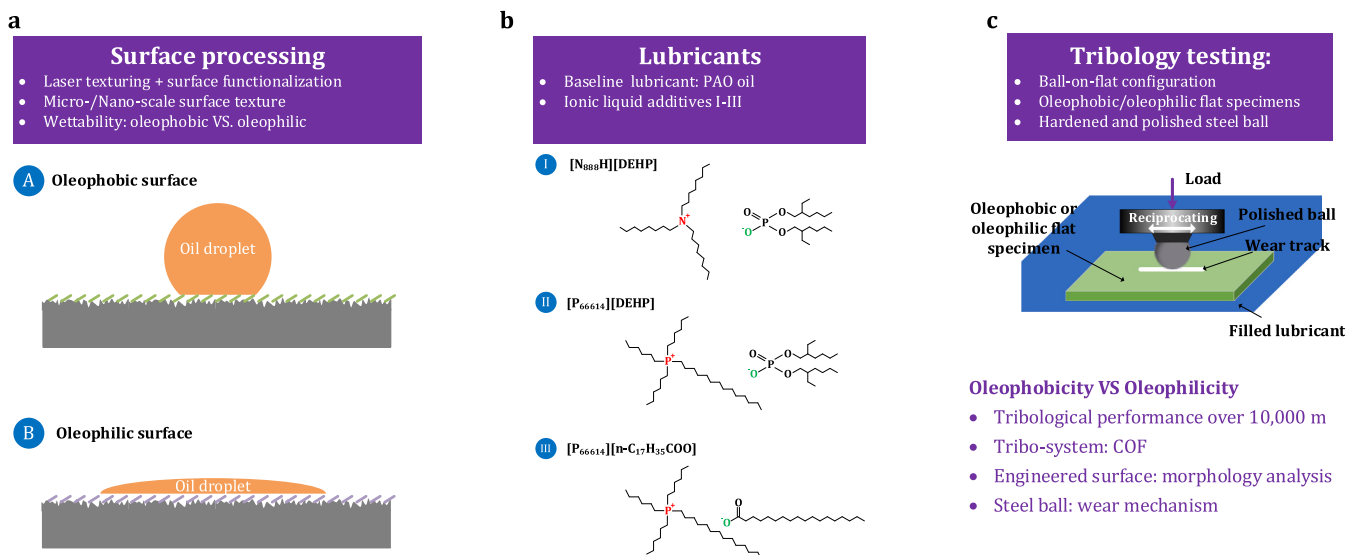

Fig. 1. Research framework of the tribology study for the engineered surfaces. (a) Oleophobic vs. oleophilic surface processing by nanostructuring surface topography and surface functionalization; (b) selected lubricants with three innovative IL additives; (c) tribology testing of the wettability-engineered flat specimens using a ball-on-flat linear reciprocating tester.

interaction between the surfaces and the lubricant. Researchers have evaluated the effect of the delta wettability, which represents wettability difference between two sliding surfaces, on tribological performance [17,18]. According to their findings, a greater delta wettability is conducive to lowering the COF and the wear rate in oil lubrication or aqueous environment. While the researchers emphasized the role of delta wettability, which is the relationship between the wettability of the ball and flat in a ball-on-flat tribo-system, the effect of wettability for the flat surface alone has also been studied [19,20]. Using dilute cutting fluids, Pang et al. [21] investigated the frictional properties of cemented carbide surfaces with various laser-induced micro-dimples and concluded that increasing hydrophilicity of the textured surface improves the COF. Huang et al. [22] examined the tribological performance of two types of PDMS surfaces, including the hydrophobic surfaces with plasma texture, and the hydrophilic surfaces without texture. The hydrophilic surfaces are found to exhibit friction coefficients that are tenths to hundredths that of the hydrophobic surfaces, suggesting that hydrophilicity is of great significance in friction reduction and lubrication enhancement. Qin et al. [23] investigated the tribological behavior of laser textured Co-Cr-Mo alloy in aqueous solution. By applying fluoro-alkyl silane treatment and various surface textures, including triangle, square and circle, the surface wettability ranging from superhydrophilicity to superhydrophobicity was achieved. They concluded that a higher contact angle leads to a larger COF. However, it is worth noting that, in these studies, the surface wettability was altered by tuning the surface texture shape and area ratio, indicating the surface morphology was not kept as constant while they compared the tribological performance of surfaces with different wettability. Therefore, the variation in friction coefficient was a result of a coupled effect of surface texture and surface wettability. To better evaluate the effect of surface wettability, it is critical to implement a systematic methodology to fabricate surfaces with varied wettability but similar morphology.

Besides the surface texture and wettability, lubricant properties are of significance in determination of tribological behavior for tribo-pair surfaces under lubrication. In the last few years, ionic liquid (IL) has emerged as an innovative additive for lubricant offering better anti-wear and tribological performance. They efficiently reduce the COF and wear on a plane surface without any textures by forming a stable protective tribo-film in the area of contact [24,25]. ILs are molten salts in ambient conditions that comprise bulky, long-chain, asymmetric cations and anions. They have inherent polarity (ions) which provide strong adsorption capability to surfaces. Compared to widely used oil lubricants, ILs have higher thermal stability, lower flammability, and lower sensitivity in rheological behavior to environmental changes [24]. Although many studies have proved the effectiveness of ILs as stand-alone lubricants, it is economically infeasible to use them standalone due to their high cost. The only feasible way to utilize their superior physiochemical properties is using them as lubricants additives. However, ILs are insoluble in most oil lubricants. In 2012, Qu et al. [26] provided the breakthrough to enhance the solubility by decreasing the ion charge density. Recently, employing ILs as oil additives has become a core theme of IL lubrication [27,28] to provide wear and friction protection. Phosphonium [29] and ammonium [30] based ILs provide superior wear and friction protection compared to other ILs. However, few research has been done on the effect of ILs for surfaces with varied wettability. It is of great importance to fill in this knowledge gap by investigating the tribological behavior of different wetting surfaces under IL-based oil lubrication.

The goal of this work is to determine the role of surface wetting on tribological behavior and elucidate the interaction between a laser-textured steel surface and ionic liquid-based oils. Through the simultaneous engineering of texture and chemistry, a unique nanosecond laser-based high-throughput surface nanostructuring (nHSN) process has been developed by the author's group [31] for metal alloys that utilizes a nanosecond laser to achieve a wide range of wetting behaviors ranging from superhydrophilicity to superhydrophobicity. This work adopts the nHSN process to the M2 tool steel alloy by nanostructuring its surface topography and functionalizing the surface wetting property relative to the lubricant oils with IL additives. As illustrated in Fig. 1, two types of surface wettability, i.e., oleophobicity and oleophilicity, but shared with the same surface texture were designed, fabricated and tested. A set of reciprocating wear tests are performed to identify the tribological properties of the tribo-system consisting of the surface-engineered, flat M2 tool steel specimen and a standard, surface-polished steel ball.

2. Experiments

2.1. Surface processing

The substrate material of interest in this work was AISI M2 tool steel as it is widely used for punches, dies and cutting tools. The M2 tool steel

Table 1
Ball-on-flat linear reciprocating testing conditions.

| Experiment	Flat surface condition	Ball condition	Lubricants
Tribo-system Exp. A	Oleophobic, nanotextured M2 steel flat surface	Hardened and polished AISI E52100 steel (ASTM A295)	PAO (with no IL additive) PAO + IL1: PAO + 1 % [N$_{888}$H] [DEHP] PAO + IL2: PAO + 1 % [P$_{66614}$] [DEHP] PAO + IL3: PAO + 1 % [P$_{66614}$][n-C$_{17}$H$_{35}$COO]
Tribo-system Exp. B	Oleophilic, nanotextured M2 steel flat surface	Hardened and polished AISI E52100 steel (ASTM A295)	PAO (with no IL additive) PAO + IL1: PAO + 1 % [N$_{888}$H] [DEHP] PAO + IL2: PAO + 1 % [P$_{66614}$] [DEHP] PAO + IL3: PAO + 1 % [P$_{66614}$][n-C$_{17}$H$_{35}$COO]
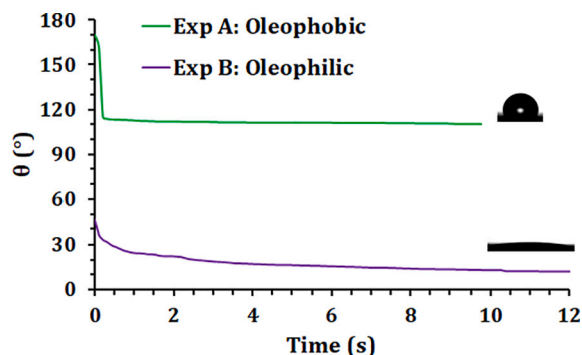
Fig. 2. Dynamic contact angle of oleophobic and oleophilic specimens with regard to PAO oil.

flat coupons were 25 mm × 25 mm × 1 mm. Before any treatment or tribological testing, these M2 tool steel coupons were ultrasonically cleaned and then air-dried.

Laser treatment and subsequent chemical treatment were applied to these M2 steel specimens to obtain the nanoscale texture and desirable chemistry. During the laser texturing step, the M2 tool steel surfaces were raster scanned with nanosecond pulse laser in water confinement. During the following chemical immersion treatment (CIT), the surfaces were submerged in the solution of ethanol with 1.5 vol% silane reagents (FOTS: 1H,1H,2H,2H-perfluorooctyltrichlorosilane; or CPTS: 3-cyano-propyltricholosilane) to obtain oleophobicity or oleophilicity respectively on the surfaces. More details about the process setup can be found in [32].

The surface topography of these treated specimens was analyzed using a Hitachi S-4800 field-emission scanning electron microscope (SEM). The surface element concentration was measured using an IXRF energy-dispersive spectroscopy (EDS) system assembled on the same SEM. The surface roughness and texture were quantitatively analyzed using a Keyence VK-X1000 confocal microscope. Dynamic change of contact angle (θ) of lubricants on these treated surfaces was measured using a contact angle goniometer (model ESr-N) at ambient conditions by micropipetting 5 μL of lubricant droplet on the treated surface and capturing the shadowgraphs using a CMOS camera.

2.2. Tribology testing

The baseline lubricant used in these tribology experiments was Mobil 1™ poly-alpha-olefin (PAO) oil. Three different ILs were selected as anti-wear additives for the PAO lubricant in this study, namely, (I) [N$_{888}$H] [DEHP]: trioctylammonium bis(2-ethylhexyl) phosphate; (II) [P$_{66614}$] [DEHP]: trihexyltetradecylphosphonium bis(2-ethylhexyl)phosphate; and (III) [P$_{66614}$][n-C$_{17}$H$_{35}$COO]: trihexyltetradecylphosphonium octa-decenoate. Fig. 1b illustrates the molecular structures of those ILs. Note IL1 is an ammonium-based IL additive, while IL2 and IL3 are phosphonium-based IL additives. The physicochemical properties of the ILs can be found in [24,25]. To make the lubricant in this work, PAO oil was mixed with 1.0 wt% IL. Such concentration has been proved to work efficiently for friction and wear reduction [24]. To improve the mixture uniformity, each lubricant sample was sonicated for 15 min before testing using a Symphony Ultrasonic Cleaner.

The tribology tests were performed on a reciprocating tribometer (Phoenix Tribology, Plint TE-77) using a ball-on-flat configuration (Fig. 1c), where a 10-mm diameter steel ball slid against the treated M2 tool steel specimens. The utilized AISI E52100 steel ball was hardened to achieve 60 HRC and polished following the ASTM A295 standard. The steel ball surface is slightly oleophilic as a droplet of PAO oil spreads uniformly on its spherical surface. However, for this work, the oil contact angle of the steel ball surface cannot be accurately determined due to the small size of this ball as well as the spherical nature of the surface. By designing these experiments using the same ball condition, the objective of this work is to determine the effect of the wettability of the flat specimen surface on the tribological behavior of the tribo-system. As part of the testing procedure, the following parameters were used: a 100 N normal force, a 10-mm stroke, a 10 Hz oscillation frequency, a 1000 m distance, and a 100 °C lubricant temperature to mimic engine normal operation temperatures [33]. The total time duration of each tribology test was 83 mins.

The ball-on-flat tribology experiments were performed following the lubricating conditions listed in Table 1. For ease of reference, the tribo-systems using the oleophobic and oleophilic specimens were designated as Exp. A and Exp. B, respectively. The COF was determined in situ by recording the tangential force and dividing it by the normal load. Before wear characterization, specimens were ultrasonically cleaned for 2 min using isopropanol alcohol. It was unfeasible to quantitatively determine the wear loss on the M2 steel flat surface due to its micro-/nanoscale roughened texture, and an analysis of alteration in surface roughness and therefore wear was performed for the specimens prior to and after the tribology tests using the confocal microscopy. The wear land of the polished steel ball was much more apparent and was quantitatively determined after these tests using a Wyko NT9100 3D optical interferometer.

3. Results & discussion

3.1. Surface characterizations prior to tribology testing

The achieved wettability of these M2 steel specimens to PAO oil was experimentally determined. As illustrated in Fig. 2, the contact angle decreases for both samples after introducing the PAO oil droplets onto the surfaces, and gradually reaches to a steady state after 10 s. The steady contact angle measured after 12 s of introducing the droplets onto the surfaces indicates that the surface processed by CPTS was oleophilicity, while the surfaces processed by FOTS showed oleophobicity. The difference in the achieved wettability was mainly due to the surface chemistry induced by the silane reagents during the CIT treatments with both specimens having similar surface roughness and nanoscale random textures. For the oleophobic surface, the FOTS molecules reduced surface energy, leading to a larger contact angle (113°), while for the oleophilic surface, the CPTS molecules have the opposite effect ($\theta \sim 13°$).
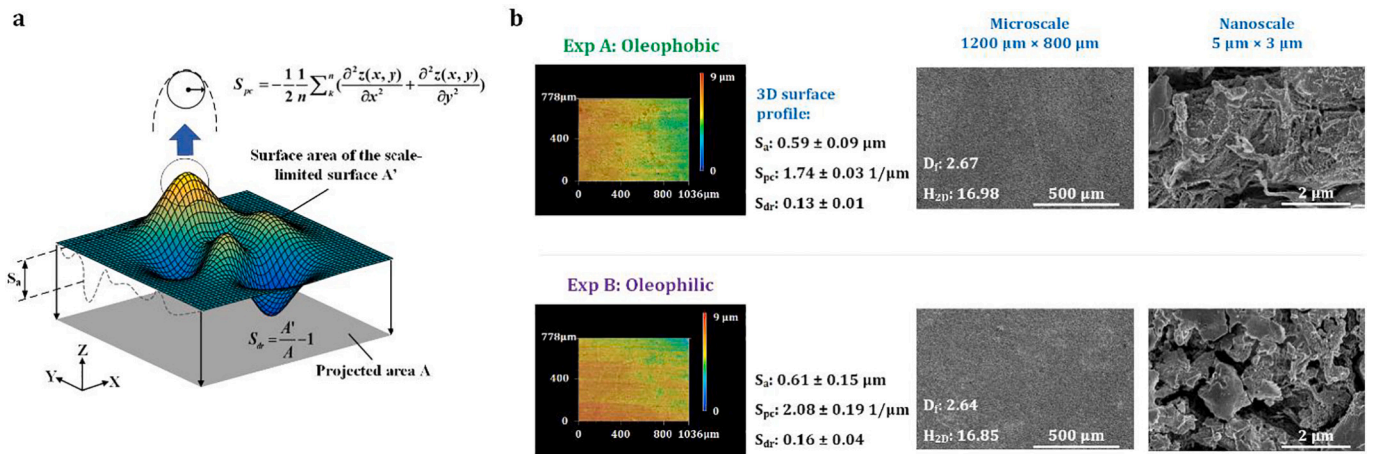
Fig. 3. Surface topography measurements (a) Schematic of surface texture parameters. (b) Surface profile and SEM micrographs of oleophobic and oleophilic surfaces at both microscale and nanoscale.
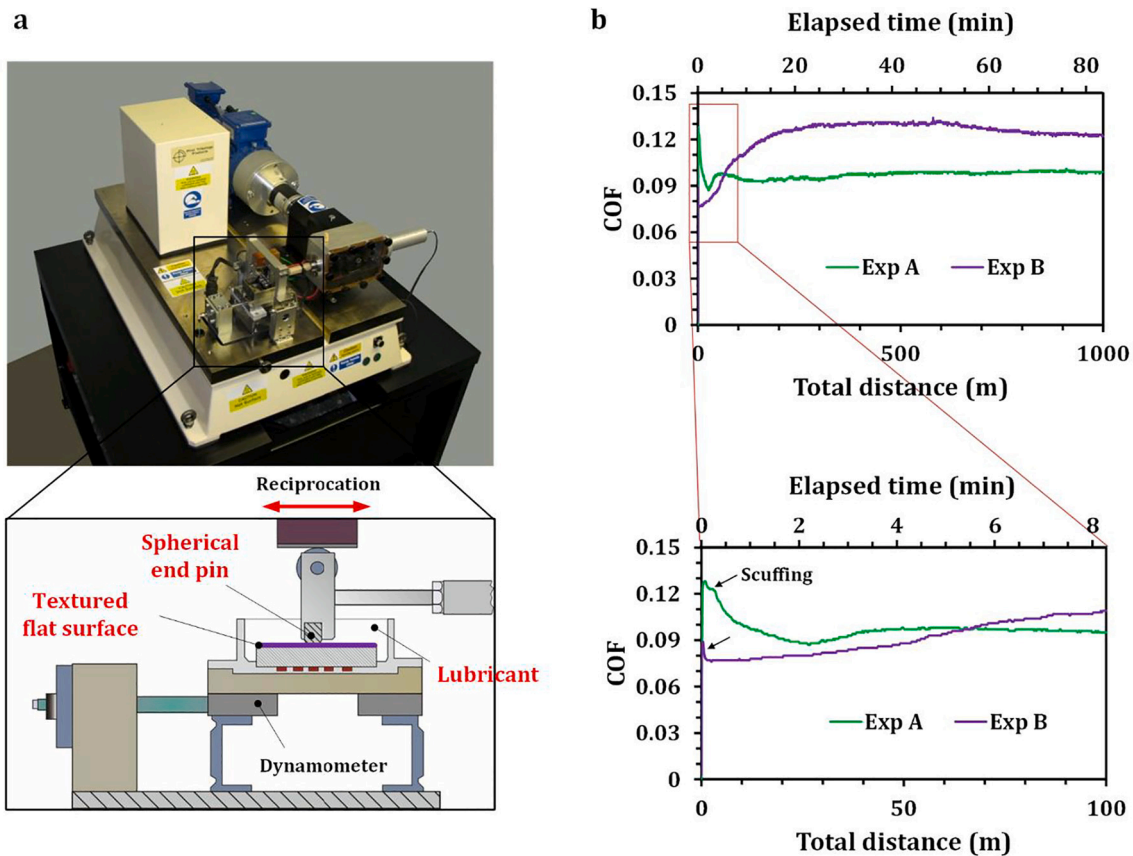

Fig. 4. The ball-on-flat tribology testing (a) experimental setup and (b) COF traces of the PAO oil for Exp A and B. Each friction trace is the average based on three repeated tests (same for the wear rate and COF results in the upcoming figures).

The surface texture measurements specified in ISO 25178 show that the oleophobic and oleophilic surfaces have similar surface texture parameters, i.e., arithmetic average height (S_a), arithmetic mean curvature of peaks (S_{pc}), and developed interfacial area ratio (S_{dr}), as schematically illustrated in Fig. 3a. S_a is expressed by:

$$S_a = \frac{1}{A}\left[\iint_A |z(x,y)|\,dxdy\right]$$ (1)

where $z(x,y)$ signifies the height deviation of point (x,y) from the

arithmetical mean of the surface, and A is the projected area [34]. S_{pc} is given by:

$$S_{pc} = -\frac{1}{2}\frac{1}{n}\sum_{k=1}^{n}\left(\frac{\partial^2 z(x,y)}{\partial x^2} + \frac{\partial^2 z(x,y)}{\partial y^2}\right)$$ (2)

where n represents the amount of peaks within the interested area [35]. A larger value of S_{pc} corresponds to sharper features, while a smaller value indicates more rounded peaks. S_{dr} is given by the ratio of the additional surface area contributed from surface textures to the area of
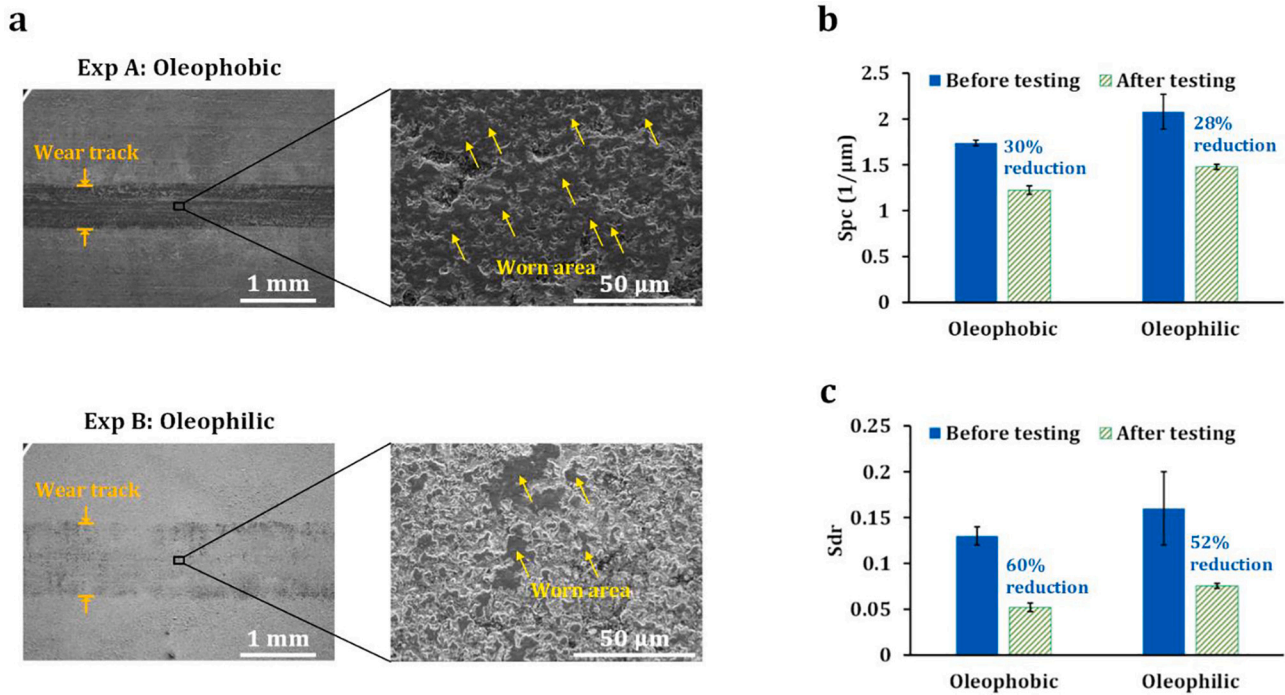
Fig. 5. Worn surface morphology of the flat specimens after tribology test in PAO oil. (a) Flat surface morphology of the oleophobic and oleophilic surfaces after tribology testing characterized using SEM. (b) S_{pc} values of the oleophobic and oleophilic surfaces before and after tribology testing. (c) S_{dr} values of the oleophobic and oleophilic surfaces before and after tribology testing.
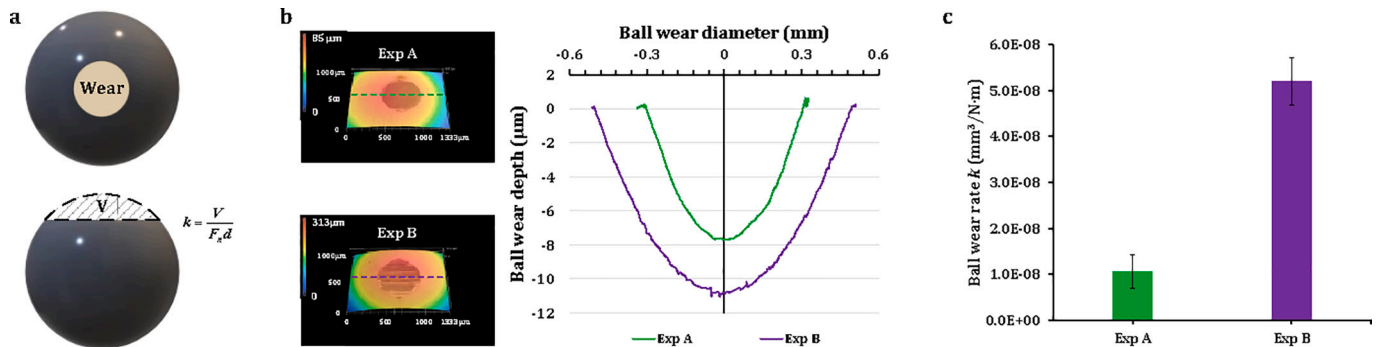

Fig. 6. (a) Schematic of wear rate calculation for the ball. (b) Worn surface and wear profile of the balls in Exp A and B for the base PAO oil. (c) k of the balls in Exp A and B for the base PAO oil.
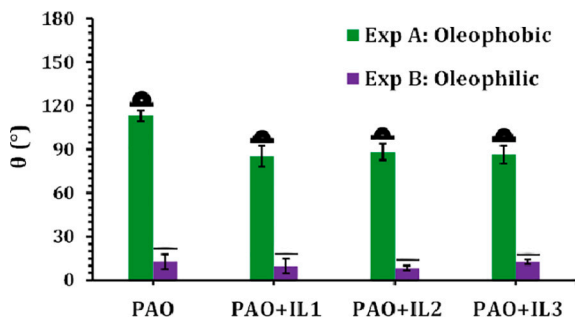

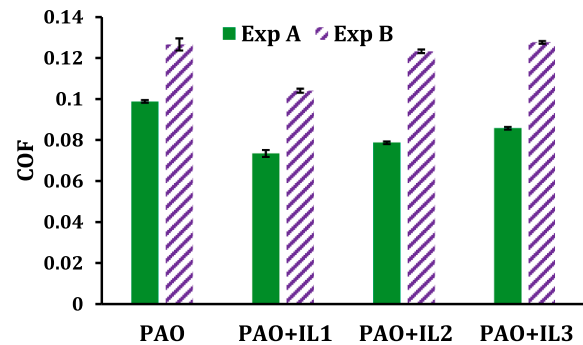**Fig. 7.** Contact angle θ for the oleophobic and oleophilic surfaces.

Fig. 8. Steady-state COF in Exp A and B measured after 500 m sliding distance.

the surface projection [34]:

$$S_{dr} = \frac{A'}{A} - 1 \tag{3}$$

where A' is the actual surface area. For each type of surface, the topography analysis was carried out on three different areas whose size is around 1 mm × 0.8 mm, and the average value of S_a, S_{pc} and S_{dr} was
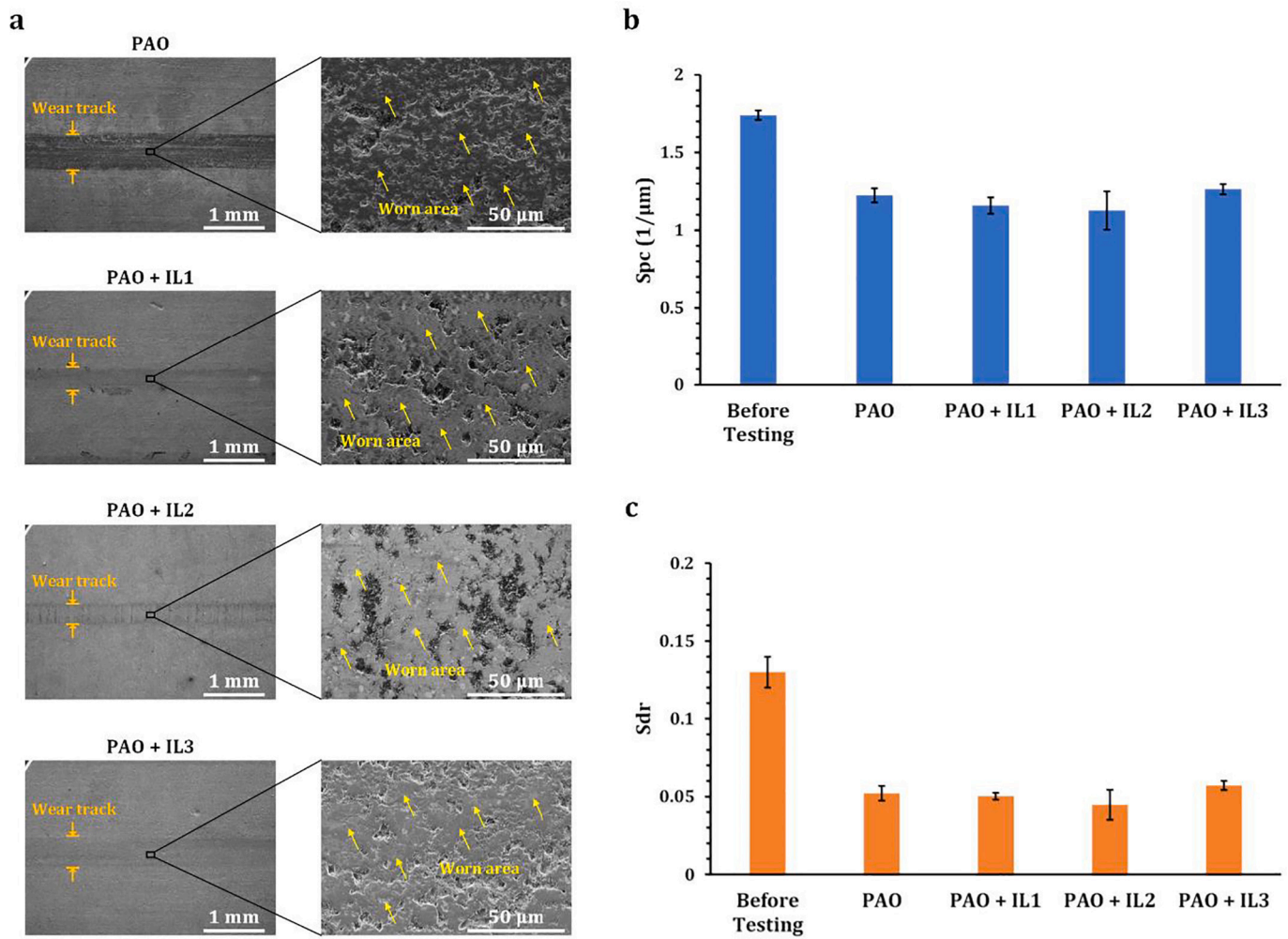
Fig. 9. Worn surface morphology for the oleophobic flat specimen in Exp A. (a) Surface morphology characterized using SEM. (b) S_{pc} values of the worn area on the oleophobic surface after tribology test in PAO oil and IL-based PAO oil. (c) S_{dr} values of the worn area on the oleophobic surface after tribology test in PAO oil and IL-based PAO oil.

Table 2
The phosphorus concentration on the worn surface in Exp. A detected using EDS.

Lubricant	Phosphorus concentration (wt%)
PAO oil	0
PAO + IL1	0.53 ± 0.05
PAO + IL2	0
PAO + IL3	0.10 ± 0.04

reported. The initial S_a of the AISI M2 tool steel specimens without any treatment is 0.31 ± 0.08 μm. As shown in Fig. 3b, the surface texture measurements resulted in an average S_a of 0.59 vs. 0.61 μm, S_{pc} of 1.74 vs. 2.08 1/μm, and S_{dr} of 0.13 vs. 0.16 for oleophobic and oleophilic surfaces, respectively, which indicate that the surface structures of the oleophobic and oleophilic surfaces have similar height, sharpness and slope. The slight difference in surface roughness can be attributed to the difference in etching effect of the FOTS and CPTS silane reagents.

The surface morphologic features were carefully examined using the SEM micrographs for the oleophobic and oleophilic surfaces prepared by the nHSN process, as shown in Fig. 3b. Both the oleophobic and oleophilic surfaces were characterized with patternless, random, nanoscale surface structures, which were created by the etching effect of the silane reagents used during the CIT process [31].

A numerical analysis of surface topography and spatial randomness

was performed to determine fractal dimension (D_f) and 2D-entropy (H_{2D}) utilizing the SEM micrographs of these textured specimens. D_f is a statistical measure of the complexity of fractals based on their self-similarity [36]. The shifting differential box-counting method [37] was used to calculate the D_f of the SEM images for the oleophobic and oleophilic surfaces. Following this method, a grey-level square image was overlapped by a 3D mesh of boxes. The D_f was then estimated by:

$$D_f = -\frac{logN_r}{logr} \qquad (4)$$

where N_r is the amount of boxes in which at least one image pixel is contained, and r is the ratio of grid size to the number of pixels contained within one side of the image. The fractal dimension quantifies the disorder and a larger value of D_f represents a higher complexity of the surface structures. H_{2D} [38] is a parameter describing the randomness of the surface structures, defined as:

$$H_{2D} = -\sum_{i=0}^{255} \sum_{j=0}^{255} p_{ij} log_2 p_{ij} \qquad (5)$$

where i is the grey level of a pixel, j represents the mean grey level of the adjacent pixels, and p_{ij} is the joint probability of a pair (i, j), which is given by the ratio of the total amount of occurrences of that pair to the total amount of pixels in the image. The similar values of D_f and H_{2D} of the oleophobic and oleophilic specimens indicate that both specimens

a

Ball wear diameter (mm)

b

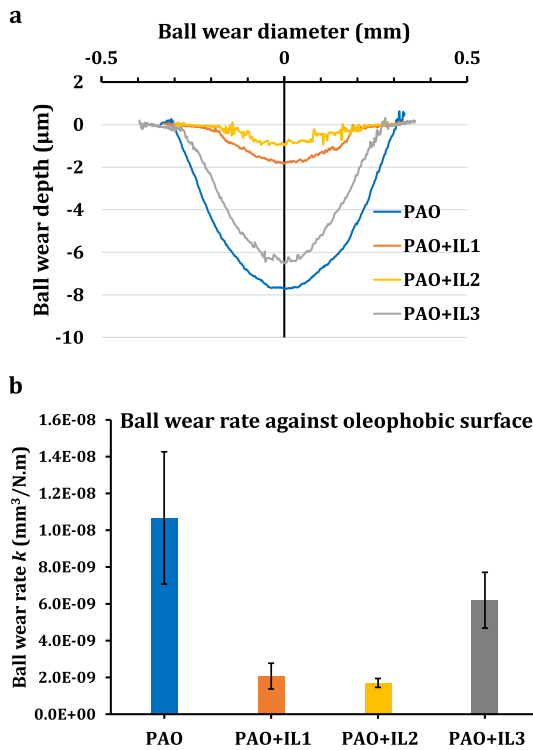**Ball wear rate against oleophobic surface**

Fig. 10. (a) Wear profile of the balls in Exp A using various lubricants. (b) Specific wear rate of the balls in Exp A measured in various lubricants.

are characterized with similar topographic complexity and spatial randomness.

The above analyses infer that both the oleophobic and oleophilic surfaces are characterized with similar surface roughness and texture with statistically similar features. Therefore, the difference in their tribological behavior is dominantly governed by the distinctive surface wettability but not surface roughness or texture.

3.2. Effect of surface wettability on the tribological behavior for PAO without IL

During the reciprocating tests, the hardened and surface-polished steel ball slid against the flat specimen under heated lubrication using PAO. The COF at the sliding interface was determined by:

$$COF = \frac{F_t}{F_n} \tag{6}$$

where F_t is the tangential force and F_n is the normal load. The progression of COF for the tribo-system Exp. A with the oleophobic surface (Fig. 4b) show that COF started from 0.06, quickly raised to 0.12, then quickly dropped, and gradually reached a steady state of about 0.1 within the first 50 m of sliding. The rapid shift of COF at the beginning indicates that a lack of lubrication may have happened locally in parts of the contact area [39]. Although Exp. B with the oleophilic surface showed a slight spike in COF at the beginning, COF increased from about 0.08 and gradually stabilized at around 0.12 after 300 m or 20 min of sliding. The steady-state COF of 0.1 in Exp. A with the oleophobic surface was relatively lower than that of 0.12 for Exp. B with the oleophilic surface. The friction coefficients fall into the range of 0.05–0.15, indicating boundary lubrication. The generally lower COF in Exp A (oleophobic) than that in Exp B (oleophilic) suggests possibility of localized micro-elastohydrodynamic lifting. For the oleophobic surface, Cassie-Baxter wetting regime [40] was achieved so that the oil did not fully penetrate the surface roughness and air was entrapped at the interface, which helped reduce the friction for the ball-flat coupling. A good level

of endurance in surface wettability was also demonstrated for both oleophobic and oleophilic specimens during these linear reciprocating tests lasting for 83 min under an elevated temperature, which suggests the nHSN processing method can be applied for industrial applications requiring surfaces with a good durability.

The SEM micrographs shown in Fig. 5a demonstrate the wear morphology of the flat specimens. For the oleophobic surface, a greater wear was observed and most nanoscale features in the wear trace were flattened due to friction wear. For the oleophilic surface, while a small portion of the wear trace can be observed, the larger area remained intact with the nanoscale structures still discernible. The surface texture parameter analysis (Fig. 5b and c) corroborated the observation. After the tribology testing, the oleophobic surface experienced a 30 % reduction in S_{pc} and 60 % reduction in S_{dr}, which indicates that the surface became flatter, and a great amount of pointed and spiky structures were flattened. In contrast, the oleophilic surface had a 28 % reduction in S_{pc} and 52 % reduction in S_{dr}, indicating that more surface structures remained intact after the testing. The feasible cause for this difference is that the PAO lubricant did not effectively contact the oleophobic surface structures, and hence the protection by the lubricant was reduced by the surface oleophobicity.

As illustrated in Fig. 6a, the ball wear rate (k) was defined as:

$$k = \frac{V}{F_n d} \tag{7}$$

where V represents the volume of ball wear, and d represents the sliding distance. In Exp. A, the diameter of wear land was around 0.6 mm while the wear diameter in Exp. B was about 1 mm. The clear difference in the k of the balls, as shown in Fig. 6c, proved the aforementioned hypothesis, that is more lubricants were expelled from the oleophobic surface so that the ball in Exp. A was better protected during the test. In Exp. B, conversely, the better lubrication condition was achieved on the oleophilic surface, leading to a smaller wear on the flat specimen.

3.3. Effects of IL additives for the tribo-system with oleophobic surface

The surface wettability was evaluated in regard to the PAO lubricants with IL additives. As shown in Fig. 7, a similar oil contact θ of around 88° was achieved for the oleophobic specimens regarding all three IL additives, which was around 25° less than the θ for the pure PAO lubricant. For the oleophilic specimens, θ around 10° was found for all three IL-based lubricants, which was 2–3° smaller than the θ for the pure PAO lubricant. In summary, the surface-engineered specimens maintained their wetting characteristics with regard to the PAO lubricants with IL additives.

The tribological performance of IL additives was investigated through ball-on-flat reciprocating tests. As illustrated in Fig. 8, all three IL additives helped reduce the steady-state COF for the tribo-system (Exp. A) with the oleophobic surface, with IL1 providing the best friction reduction. For tribo-system Exp. B with the oleophilic surface, ammonium-based IL1 additive still reduced the COF, while the phosphonium-based ILs (IL2 and IL3) provided little improvement in friction. It is worth noting that the tribological performance of the tribo-system is a coupled effect of surface conditions with lubricant properties. For each lubricant, Exp. A exhibited the lower COF than Exp. B, indicating that surface oleophobicity leads to friction reduction when other conditions are the same. When comparing PAO base oil with PAO + ILs, although the surface oleophobicity was weakened, the IL additives were capable of improving the tribological performance of the tribo-system.

The wear scar morphology is shown in Fig. 9a. A slight improvement of the wear performance of the oleophobic surface can be observed for IL additives. Under a low magnification on the left side, it can be seen that PAO without IL additive gives the widest wear track, while the wear tracks become much narrower for IL1 and IL2. The IL3 leads to a wear
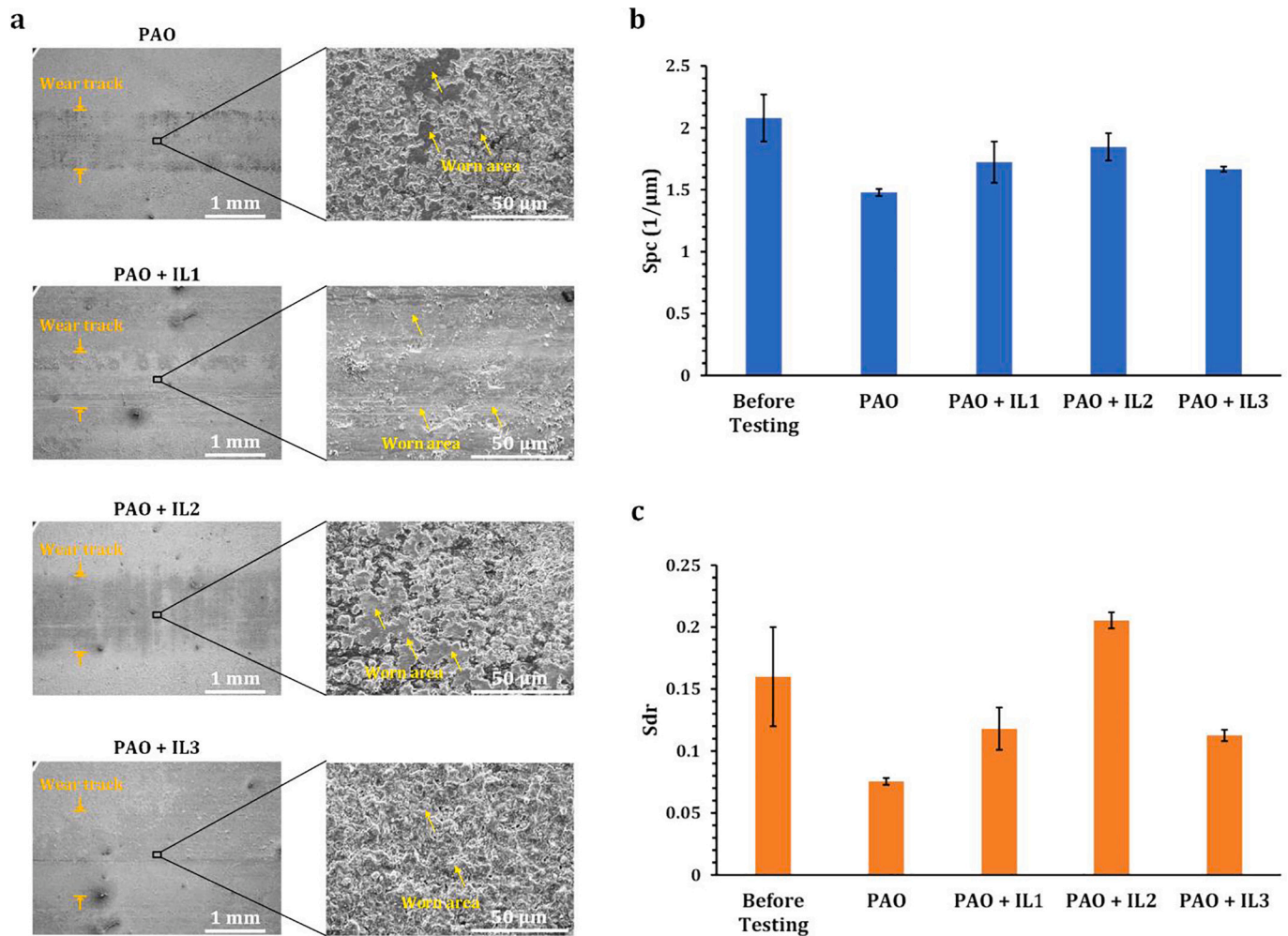
Fig. 11. Worn surface morphology for the oleophilic flat in Exp B. (a) Oleophilic surface morphology characterized using SEM. (b) S_{pc} values of the worn area on the oleophilic surface after tribology testing in PAO oil and IL-based PAO oil. (c) S_{dr} values of the worn area on the oleophilic surface after tribology testing in PAO oil and IL-based PAO oil.

Table 3
The phosphorus concentration on the worn surface in Exp. B detected using EDS.

Lubricant	Phosphorus concentration (wt%)
PAO oil	0
PAO + IL1	0.87 ± 0.08
PAO + IL2	0.69 ± 0.06
PAO + IL3	0.12 ± 0.05

track slightly narrower than the PAO alone but wider than the other two ILs. Under a high magnification, the worn surface morphology for PAO oil and IL-based PAO oils are similar with each other. Most of the areas are worn to flat for all four lubricants. The surface topography measurements of the worn area confirmed the observation from these SEM images. The result (Fig. 9b) shows that all four lubricants give a similar worn surface topography. The S_{pc} and S_{dr} values are very similar for the four cases, indicating that the worn surfaces have similar roughness and similar surface structures.

The chemistry of the surface after the tribology testing was analyzed using EDS. Phosphorus was used as an indicator of the presence of ILs on the surface, as all the ILs used in the study contain phosphorus in their cations and/or anions as shown in Fig. 1. The direct tribo-chemical reaction between the metallic contact surface and chemical deposition of the IL additives will lead to a P-rich tribo-film on top of the steel

substrate [41]. The result (Table 2) shows that the worn surfaces for IL1 and IL3 only contained tiny amount of phosphorus. For IL2, the phosphorus concentration of the worn surface is even lower than the detection limit of EDS. The result indicates that the IL additives cannot effectively form the tribo-film on the oleophobic surface, which is why the wear protection is inefficient for the flat surface.

The flat surfaces tend to repel the lubricants towards the ball due to the oleophobicity of the flats. Therefore, to better demonstrate the effect of IL additives, the ball wear was measured. Fig. 10a shows the wear morphology and wear profile on the ball. The wear is reduced after adding ILs to the PAO oil. The specific wear rate results (Fig. 10b) show that all the three ILs provide superior wear protection for the ball, among which IL2 gives the best wear protection. The wear rate results of the balls provide an indirect way to evaluate the effect of adding IL additives. A possible explanation for the wear rate reduction of the balls is the tribo-film formation on the balls, which is yet to be confirmed. In the next section, the chemistry analysis on the flat surfaces supported the hypothesis of tribo-film formation on the flats.

3.4. Effects of IL additives for the tribo-system with oleophilic surface

For the tribo-system Exp. B with oleophilic surface, morphology of the worn area on the flat surfaces was analyzed. The corresponding ball wear rate was measured and shown in Fig. S1. For the flat surface, shallower wear track was observed from Fig. 11a, and the worn part was

more scattered after ILs were added. The surface topography measurement (Fig. 11b) demonstrates that all the ILs show better wear protection in comparison with the PAO oil without IL additives. The surface tested in PAO + IL2 lubrication has the largest S_{pc} and S_{dr} values, indicating that the surface microstructures were best preserved during the test. The average value of S_{dr} for the surface under PAO + IL2 lubrication is larger than the surface before testing. This is due to the relatively large roughness variation of the oleophilic surface before testing, resulting from the nonuniformity of the etching effect of CPTS.

The difference in wear results of Exp. B from Exp. A is due to the oleophilicity of the flat surface. As the surface is oleophilic, the lubricant was able to better attach the surface and the IL additives can form the tribo-film more efficiently during the test, therefore leading to wear protection on the surface. The EDS result listed in Table 3 confirmed it by showing the phosphorus concentration on the worn area of the oleophilic surface after the testing. The worn surfaces contain 0.87 wt%, 0.69 wt% and 0.12 wt% phosphorus after testing using PAO + IL1, PAO + IL2 and PAO + IL3, respectively, which are all higher than the corresponding oleophobic surfaces in Exp. A. The best wear protection is achieved in PAO + IL2 lubrication, while the IL1 shows the largest amount of phosphorus. This discrepancy is possibly due to the limitations of EDS technique. As the specimen surfaces are rough (feature size is much larger than the wavelength of incident and exiting radiation for EDS), the micro-asperities on surface would induce interference and uncertainties to reduce the precision of EDS quantitative analysis.

4. Conclusions

In this study, the surface wettability impact was experimentally evaluated for the tribo-system consisting of the wettability-engineered, flat steel specimen, the standard, polished steel ball, and ionic liquid-based lubricants. The research concludes the following:

1. The tribo-system consisting of an oleophobic flat steel specimen delivers a lower COF compared with the one using the oleophilic flat specimen. The steady-state COF for the oleophobic group ranges from 0.07 to 0.10 for PAO oil and IL-based PAO oil lubrications, while for the oleophilic group the steady-state COF ranges from 0.10 to 0.12.
2. All three selected IL additives help reduce the COF. Particularly, the ammonium-based IL additive gives the best friction reduction.
3. When IL is added, the wear rate becomes lower for the polished steel ball under the tribo-system with the oleophobic flat specimen. Among all the IL additives, the phosphonium-based IL2 ([P$_{66614}$] [DEHP]) leads to the lowest wear rate for the ball.
4. Less wear occurs to the oleophilic flat surface than the oleophobic surface for the lubricants tested in this work. The oleophilic surface fosters the formation of P-rich tribo-film from IL additives and is hence better protected by the lubricants.
5. All three IL additives improve wear protection for the oleophilic flat steel specimen, among which the phosphonium-based IL2 is most effective.

Declaration of competing interest

The authors declare the following financial interests/personal relationships which may be considered as potential competing interests: Hongtao Ding reports financial support was provided by National Science Foundation.

Acknowledgement

Appendix A. Supplementary data

Supplementary data to this article can be found online at https://doi.org/10.1016/j.jmapro.2023.04.031.

References

[1] Carpick RW, Jackson A, Sawyer WG, Argibay N, Lee P, Pachon A, et al. The tribology opportunities study: can tribology save a quad? Tribol Lubr Technol 2016;72:44.

[2] Hemanth G, Suresha B, Ananthapadmanabha. Hybrid and electric vehicle tribology: a review. Surf Topogr Metrol Prop 2021;9. https://doi.org/10.1088/2051-672X/ac2bf6.

[3] Sanchez Garrido D, Leventini S, Martini A. Effect of temperature and surface roughness on the tribological behavior of electric motor greases for hybrid bearing materials. Lubricants 2021;9. https://doi.org/10.3390/lubricants9060059.

[4] Becker EP. Lubrication and electric vehicles. Tribol Lubr Technol 2019;75:60.

[5] Bhaduri D, Batal A, Dimov SS, Zhang Z, Dong H, Fallqvist M, et al. On design and tribological behaviour of laser textured surfaces. Procedia CIRP 2017;60:20–5. https://doi.org/10.1016/j.procir.2017.02.050.

[6] Dunn A, Wlodarczyk KL, Carstensen JV, Hansen EB, Gabzdyl J, Harrison PM, et al. Laser surface texturing for high friction contacts. Appl Surf Sci 2015;357:2313–9. https://doi.org/10.1016/j.apsusc.2015.09.233.

[7] Ahmed YS, Paiva JM, Arif AFM, Amorim FL, Torres RD, Veldhuis SC. The effect of laser micro-scale textured tools on the tool-chip interface performance and surface integrity during austenitic stainless-steel turning. Appl Surf Sci 2020;510:145455.

[8] Zhang K, Zhang C, Li H, Dong B, Guo X, Liu Y. Study on the substrate surface micro-texturing/carburizing regulating the film-substrate adhesion and wear behavior of DLC coatings. DiamRelat Mater 2022;130:109535.

[9] Ma J, Liu Y, Zhang N, Zhang W. Wettability transition and tribological properties of hydrophobic alloy surfaces prepared by one-step method. Tribol Int 2023;178: 108020.

[10] Voyer J, Ausserer F, Klein S, Velkavrh I, Diem A. Reduction of the adhesive friction of elastomers through laser texturing of injection molds. Lubricants 2017;5:45. https://doi.org/10.3390/lubricants5040045.

[11] Zhao Q-Z, Wang Z. Manipulation of tribological properties of metals by ultrashort pulsed laser micro-/nanostructuring. IntechOpen; 2016.

[12] Wei S, Shang H, Liao C, Huang J, Shi B. Tribology performance of surface texturing plunger. Biomimetics 2019;4:54.

[13] Kasem H, Stav O, Grützmacher P, Gachot C. Effect of low depth surface texturing on friction reduction in lubricated sliding contact. Lubricants 2018;6:62. https://doi.org/10.3390/lubricants6030062.

[14] Hu T, Hu L. The study of tribological properties of laser-textured surface of 2024 aluminium alloy under boundary lubrication. Lubr Sci 2012;24:84–93. https://doi.org/10.1002/ls.

[15] Lu P, Wood RJK, Gee MG, Wang L, Pfleging W. The friction reducing effect of square-shaped surface textures under lubricated line-contacts—an experimental study. Lubricants 2012;4:26. https://doi.org/10.3390/lubricants4030026.

[16] Hsu SM, Jing Y, Hua D, Zhang H. Friction reduction using discrete surface textures: principle and design. J Phys D Appl Phys 2014;47:335307. https://doi.org/10.1088/0022-3727/47/33/335307.

[17] Borruto A, Crivellone G, Marani F. Influence of surface wettability on friction and wear tests. Wear 1998;222:57–65.

[18] Pawlak Z, Urbaniak W, Oloyede A. The relationship between friction and wettability in aqueous environment. Wear 2011;271:1745–9. https://doi.org/10.1016/j.wear.2010.12.084.

[19] Seid Ahmed Y, DePaiva JM, Amorim FL, Torres RD, de Rossi W, Veldhuis SC. Laser surface texturing and characterization of austenitic stainless steel for the improvement of its surface properties. Int J Adv Manuf Technol 2021;115: 1795–808.

[20] Duan Z, Chen L, Li B. Effect of micro-textured morphology with different wettabilities on tool cutting performance. Int J Adv Manuf Technol 2022;123: 1745–54.

[21] Pang M, Liu X, Liu K. Effect of wettability on the friction of a laser-textured cemented carbide surface in dilute cutting fluid. Adv Mech Eng 2017;9:1–9. https://doi.org/10.1177/1687814017738154.

[22] Huang W, Jiang L, Zhou C, Wang X. The lubricant retaining effect of micro-dimples on the sliding surface of PDMS. Tribol Int 2012;52:87–93. https://doi.org/10.1016/j.triboint.2012.03.003.

[23] Qin L, Lin P, Zhang Y, Dong G, Zeng Q. Influence of surface wettability on the tribological properties of laser textured Co-Cr-Mo alloy in aqueous bovine serum albumin solution. Appl Surf Sci 2013;268:79–86. https://doi.org/10.1016/j.apsusc.2012.12.003.

[24] Zhou Y, Qu J. Ionic liquids as lubricant additives: a review. ACS Appl Mater Interfaces 2017;9:3209–22. https://doi.org/10.1021/acsami.6b12489.

[25] Barnhill WC, Luo H, Meyer HM, Ma C, Chi M, Papke BL, et al. Tertiary and quaternary ammonium-phosphate ionic liquids as lubricant additives. Tribol Lett 2016;63:22. https://doi.org/10.1007/s11249-016-0707-6.

[26] Qu J, Bansal DG, Yu B, Howe JY, Luo H, Dai S, et al. Antiwear performance and mechanism of an oil-miscible ionic liquid as a lubricant additive. ACS Appl Mater Interfaces 2012;4:997–1002. https://doi.org/10.1021/am201646k.

[27] Singh J, Chatha SS, Bhatia R. Behaviour and applications of ionic liquids as lubricants in tribology: a review. Mater Today Proc 2022;56:2659–65.

[28] Reeves CJ, Kasar AK, Menezes PL. Tribological performance of environmental friendly ionic liquids for high-temperature applications. J Clean Prod 2021;279: 123666.

[29] Rahman MH, Khajeh A, Panwar P, Patel M, Martini A, Menezes PL. Recent progress on phosphonium-based room temperature ionic liquids: synthesis, properties, tribological performances and applications. Tribol Int 2022;167:107331.

[30] Guo H, Iglesias P. Tribological behavior of ammonium-based protic ionic liquid as lubricant additive. Friction 2021;9:169–78.

[31] Wang Q, Samanta A, Shaw SK, Hu H, Ding H. Nanosecond laser-based high-throughput surface nanostructuring (nHSN). Appl Surf Sci 2020;507:145136. https://doi.org/10.1016/j.apsusc.2019.145136.

[32] Huang W, Nelson B, Tian S, Ordikhani-Seyedlar R, Auyeung RCY, Samanta A, et al. Superhydrophobic surface processing for metal 3D printed parts. Appl Mater Today 2022;29:101630. https://doi.org/10.1016/J.APMT.2022.101630.

[33] Qu J, Luo H, Chi M, Ma C, Blau PJ, Dai S, et al. Comparison of an oil-miscible ionic liquid and ZDDP as a lubricant anti-wear additive. Tribol Int 2014;71:88–97. https://doi.org/10.1016/j.triboint.2013.11.010.

[34] Dai Q, Li M, Khonsari MM, Huang W, Wang X. The thermocapillary migration on rough surfaces. Lubr Sci 2019;31:163–70.

[35] Hu L, Yun D, Gao J, Tang C. Monitoring and optimizing the surface roughness of high friction exposed aggregate cement concrete in exposure process. Constr Build Mater 2020;230:117005.

[36] Mandelbrot BB, Wheeler JA. The fractal geometry of nature. Am J Phys 1983;51: 286–7. https://doi.org/10.1119/1.13295.

[37] Chen W-S, Yuan S-Y, Hsieh C-M. Two algorithms to estimate fractal dimension of gray-level images. Opt Eng 2003;42:2452. https://doi.org/10.1117/1.1585061.

[38] Huang W, Samanta A, Chen Y, Baek S, Shaw SK, Ding H. Machine learning model for understanding laser superhydrophobic surface functionalization. J Manuf Process 2021;69:491–502. https://doi.org/10.1016/J.JMAPRO.2021.08.007.

[39] Odi-Owei S, Roylance BJ, Xie LZ. An experimental study of initial scuffing and recovery in sliding wear using a four-ball machine. Wear 1987;117:267–87.

[40] Cassie ABD, Baxter S. Wettability of porous surfaces. Trans Faraday Soc 1944;40: 546–51. https://doi.org/10.1039/TF9444000546.

[41] Zhou Y, Leonard DN, Guo W, Qu J. Understanding tribofilm formation mechanisms in ionic liquid lubrication. Sci Rep 2017;7:8426. https://doi.org/10.1038/s41598-017-09029-z.